Chalcogenide Letters Vol. 16, No. 9, September 2019, p. 449 - 455

THE EFFECT OF Cu-DOPING ON THE STRUCTURAL, MICROSTRUCTURAL, OPTICAL, AND ELECTRICAL PROPERTIES OF Sb_2S_3 THIN FILMS

U. CHALAPATHI, B. POORNAPRAKASH, S. H. PARK*
Department of Electronic Engineering, Yeungnam University, Gyeongsan 38541, South Korea

The un-doped and Cu-doped (1.3-8.7 at%) Sb2S3 thin films are prepared by an easy and low-cost chemical bath deposition method and annealing at 250 °C under Ar ambiance. The X-ray diffraction studies revealed that the un-doped and Cu-doped Sb2S3 films exhibit polycrystalline nature with orthorhombic crystal structure. The crystallite size of the films increased up to a Cu-doping concentration of 2.0 at% and a slight decrease beyond 4 at%. Raman spectra of the films confirms the formation of single phase Sb2S3 up to 2 at% and the emergence of minor CuSbS2 phase beyond 4 at% Cu-doping concentration. Field emission scanning electron microscopy studies revealed the transformation of round shaped grain morphology to a smooth, dense and compact film formation with increasing Cu-doping concentration. The direct optical band gaps of the pure and Cu-doped Sb2S3 films are in the range of 1.70-1.72 eV. The electrical conductivity of the films is found to be p-type, and the electrical resistivity decreases, and carrier concentration of the films increases with increasing Cu-doping concentration in the films.

(Received June 4, 2019; Accepted September 17, 2019)

Keywords: Sb2S3 thin films, Cu-doping, Annealing, Raman spectroscopy, Electrical properties

1. Introduction

In view of its potential applications in the emerging fields of science and technology such as thermoelectric devices, photodetectors, microwave devices, and solar cells, Sb2S3 has attracted remarkable attention from the past few decades [1-4]. The suitable optoelectronic properties such as the direct optical band gap 1.7 eV, optical absorption coefficient $>10^4$ cm^{-1}, p-type conductivity nature and earth-abundant and non-toxic precursor elements made Sb2S3 as an appropriate absorber layer for mesosuperstructured (MS) and planar-heterojunction (PHJ) solar cells. The Sb2S3-based solar cells exhibited a maximum conversion efficiency of 7.5% in the MS structure [5], and 4.3% in the PHJ structure [6]. Several methods of depositing Sb2S3 thin films including evaporation [7], sputtering [8], spray pyrolysis [9, 10], electrodeposition [11, 12], and chemical bath deposition [1, 2, 4, 13, 14] have been investigated. Sb2S3 possesses high electrical resistivity, which is the reason why the solar cells based on Sb2S3 showed lower device efficiency. Controlling the conduction type and obtaining low resistive Sb2S3 layers is very much essential to increase the efficiency of these cells. In this connection, several impurities such as Ag, Sn, C, Zn, Ti, and Bi were doped into Sb2S3 thin films [15-20]. In our previous report, we have grown Sn-doped Sb2S3 films by chemical bath deposition [20], and the results showed the formation of large-grained Sb2S3 films with decreased electrical resistivity. Recently, Cu-doped Sb2S3 reported by Valentina Janosevic et al. improved the performance of Sb2S3-based solar cells to 8% [21]. These results motivated us to deposit Cu-doped Sb_2S_3 films and study its effect on the growth and properties of Sb2S3 films prepared by chemical bath deposition, a simple, inexpensive, and large area deposition method.

*Corresponding author: sihyun_park@ynu.ac.kr

2. Experimental details

For the preparation of un-doped and Cu-doped Sb2S3 (1.3-8.7 at%) thin films, SbCl3, Na2S2O3, and ethylenediamine tetraacetic acid (EDTA) were used as the starting chemicals. The deposition of un-doped Sb2S3 films involves the mixing of, 2.28 g of SbCl3 dissolved in 5 mL of acetone, 2.5 mL of 0.5 M EDTA, 20 mL of 1 M Na2S2O3, and sufficient amount of DI water, to make a 100 mL solution. Like-wise, the deposition of Cu-doped Sb2S3 films involves the mixing of, appropriate amounts of SbCl3, CuCl2.2H2O dissolved in 5 mL of acetone, 2.5 mL of 0.5 M EDTA, 20 mL of 1 M Na2S2O3, and the sufficient amount of DI water. The deposition conditions such as the bath temperature of 40 ^{o}C and deposition time of 3 h are alike to the conditions used in our previous reports for Sb2S3 and Sn-doped Sb2S3 thin films [20, 22]. The as obtained pure and Cu-doped Sb2S3 films were annealed at 250 ^{o}C for 30 min in a quartz furnace with Ar gas inserting up to atmospheric pressure [20, 22].

The structural properties of the films were studied by recording the GIXRD patterns of the films on a PANalytical XRD using Cu Kα radiation (λ = 0.15406 nm) and a glancing angle of (ω) of 3°. The phase analysis of the films has been carried out by recording the Raman spectra of the films using a Thermo Fisher Scientific (Nicolet 6700) confocal Raman spectrometer using a 532 nm laser source. Field emission scanning electron microscopy (FESEM, Hitachi, S-4100) was used to probe the surface morphology and thickness of the films. Energy-dispersive X-ray spectroscopy (EDS) coupled with FESEM was used to measure the elemental composition of the films. An UV-Vis-NIR double beam spectrophotometer (Cary 5000) was used to record the transmittance data of the films, and a Hall measurement unit (EUCOPIA; HMS-3000) was used to measure the electrical properties of the films.

3. Results and discussion

3.1. Elemental composition

The elemental compositions of the pure and Cu-doped Sb2S3 thin films are listed in Table 1. From the table it is seen that the elemental composition of the pure Sb2S3 films slightly deviated from the stoichiometry and showed Sb-rich and S-poor composition (the stoichiometric composition is Sb = 40, and S = 60 at%). On increasing the CuCl2.2H2O concentration and correspondingly decreasing the SbCl3 concentration in the solution, the Cu-doping concentration has been increased from 1.3 to 8.7 at%, whereas a proportionate reduction in the Sb at% was observed. The composition of the films is mostly S-poor and Sb-rich contemplating the error limits of EDS.

Table 1. Composition data of the pure and Cu-doped Sb2S3 films.

S.No.	Atomic percentage		
	Sb	S	Cu
1	46.4	53.6	0.0
2	46.3	52.4	1.3
3	46.2	51.6	2.0
4	45.2	50.8	4.0
5	43.2	51.1	5.8
6	39.9	51.4	8.7

3.2. Structural analysis

3.2.1. X-ray diffraction

The XRD spectra of the pure and Cu-doped Sb2S3 films are presented in Fig. 1. The un-doped Sb2S3 film XRD pattern show diffraction peaks at positions clearly coinciding the standard diffraction peak positions of Sb2S3 film (JCPDS card no. 42-1393). The films are found to exhibit

orthorhombic crystal structure with lattice parameters a = 1.142 nm, b = 0.381 nm, and c = 1.124 nm, which are close to the standard values of Sb2S3. The Cu-doping into Sb2S3 films did not show any change in the XRD peak positions indicating that the films are Sb2S3. However, the peaks become sharp and the intensity increases up to 2.0 at% of Cu-doping. The peaks become broader, the intensity of the peaks decreases and a small hump marked with `*' symbol was observed beyond 4.0 at% of Cu-doping. The sharp diffraction peaks until 2.0 at% of Cu-doping indicates an improvement in the crystallinity of the films with increasing Cu-doping percentage. The decreased peak intensity and increased peak broadening of the films beyond 4.0 at% of Cu-doping could be due to the decreased films thickness (thickness decreased from 700 to 600 nm). The presence of a small hump at 29.90^o is due to the CuSbS2 phase (JCPDS Card No. 44-1417), indicating that $CuSbS_2$ phase is forming from 4 at% of Cu-doping in Sb2S3 films.

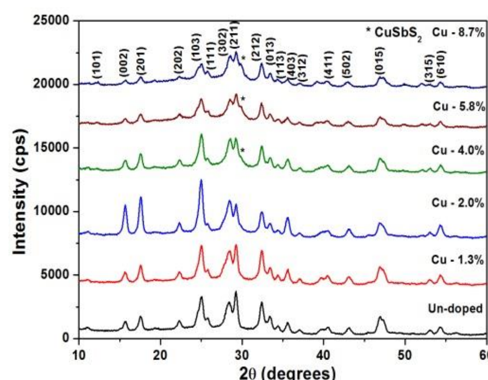

Fig. 1. XRD spectra of the pure and Cu-doped Sb_2S_3 thin films.

3.2.2. Raman spectroscopy

Raman spectroscopy has been used a complementary tool for phase analysis, and Fig. 2 shows the Raman spectra of the pure and Cu-doped Sb2S3 films. The un-doped Sb2S3 film Raman spectrum shows the modes at 132, 160, 193, 241, 286, and 310 cm^{-1}, the intense being at 286, and 310 cm^{-1}, which are matching the reported Raman modes of Sb2S3 at positions 305, 280, 236, 189, 155 and 125 cm^{-1} [23, 24]. The slight difference in observed peak positions than the reported peaks could be due to variations in the composition or crystallinity. The Raman spectra of the Cu-doped Sb2S3 films up to 2.0 at% showed the similar modes as that of the un-doped Sb2S3. However, the increased Cu-doping concentration from 4 at% to 8.7 at% resulted in the emergence of additional peak at 338 cm^{-1} along with the modes of Sb2S3. The new peak observed at 338 cm^{-1} is due to the CuSbS2 phase [25-27], which appeared as a secondary phase from XRD analysis. This indicates that the XRD and Raman studies confirmed the formation of CuSbS2 secondary phase with more than 4 at% of Cu-doping concentration in the films.

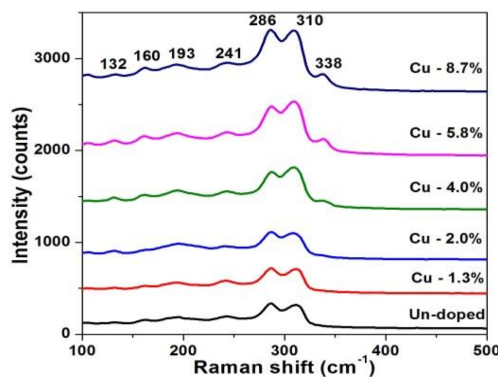

Fig. 2. Raman spectra of the pure and Cu-doped Sb2S3 thin films.

3.3. Microstructure

The microstructures of the un-doped and Cu-doped Sb2S3 thin films recorded by FESEM are presented in Fig. 3. The microstructure of the un-doped Sb2S3 film contains the round-shaped grains uniformly distributed over the film surface with a compact grain structure. The Cu-doping into Sb2S3 showed significant changes in the morphology of the films. The round-shaped grain morphology has been disappeared, and a smooth and compact surface morphology has been evolved with a Cu-doping of 1.3 at%. The compactness and surface smoothness of the films increased with increasing Cu-doping concentration from 2 at% to 4 at%. Further increasing the Cu-doping concentration from 5.8 to 8.7 at% resulted in the formation of fine-grained compact morphology. Thus, the Cu-doping in the Sb2S3 films promoted the compact and smooth surface morphology.

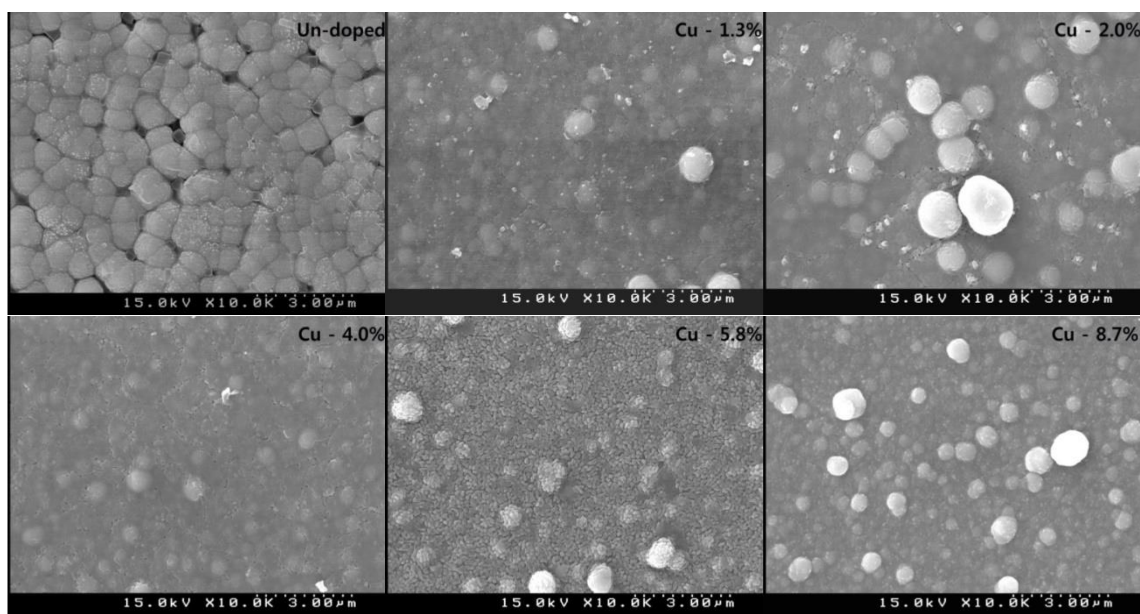

Fig. 3. FESEM images of the pure and Cu-doped Sb2S3 thin films.

3.4. Optical absorption

Fig. 4 shows the transmittance spectra of the pure and Cu-doped Sb2S3 thin films recorded in the wavelength range of 300-2500 nm. The transmittance spectrum of the pure Sb2S3 film exhibits a transmittance of ~50% at higher wavelengths and an onset of absorption at 760 nm, which is close to the reported onset of fundamental absorption edge of Sb2S3 [28]. By doping Cu in to the films, no change in the onset of absorption and an increase in the transmittance of the films are observed. The increased transmittance of the films could be due to the increased crystallinity as well as the decreased thickness of the films.

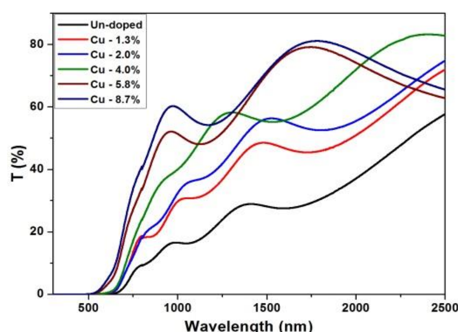

Fig. 4. Transmittance spectra of the pure and Cu-doped Sb2S3 thin films.

The direct optical band gap of the pure and Cu-doped Sb2S3 thin films was determined with the help of the $(\alpha h\gamma)^2$ versus hγ curves. The $(\alpha h\gamma)^2$ versus hγ curves of the pure and Cu-doped Sb2S3 are shown in Fig. 5. The uncertainty in the determination of the optical band gap is ±0.02 eV. The direct optical band gaps of the pure and Cu-doped Sb2S3 thin films are in the range of 1.70-1.72 eV, which are close to the reported direct band gap value of Sb2S3 [20, 28].

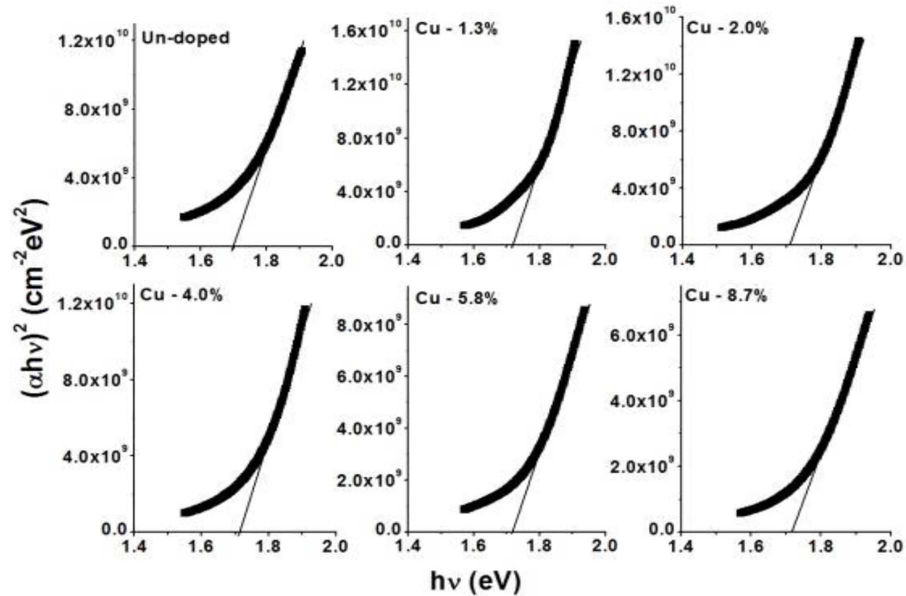

Fig. 5. $(\alpha h\gamma)^2$ *versus hγ curves of the pure and Cu-doped Sb2S3 thin films.*

3.5. Electrical properties

The electrical properties of the un-doped and Cu-doped Sb2S3 thin films were determined using Hall Effect at room temperature. The un-doped and doped Sb2S3 films showed p-type electrical conductivity. The electrical resistivity, hole mobility, and carrier concentration of the un-doped Sb2S3 films are found to be $2.0x10^5$ Ωcm, 1.0 $cm^2V^{-1}s^{-1}$, and $2.7x10^{13}$ cm^{-3}, respectively. The electrical resistivity of the films decreased from $2.0x10^5$ to $0.2x10^4$ Ωcm, and carrier concentration of the films increased from $2.7x10^{13}$ to $9.6x10^{14}$ cm^{-3} with increasing the Cu-doping concentration from 1.3 to 8.7 at%. The hole mobility of the films did not show a systematic change in its value with increasing Cu-doping concentration in the films.

Table 2. Electrical properties of the pure and Cu-doped Sb2S3 thin films.

Cu-doping%	Electrical properties		
	Resistivity (Ωcm)	Mobility ($cm^2V^{-1}s^{-1}$)	Carrier concentration (cm^{-3})
0	$2.0x10^5$	1.0	$2.7x10^{13}$
1.3	$1.8x10^5$	1.2	$1.3x10^{13}$
2.0	$1.9x10^5$	5.2	$5.4x10^{13}$
4.0	$1.0x10^5$	2.3	$8.7x10^{13}$
5.8	$1.7x10^4$	3.2	$1.1x10^{14}$
8.7	$0.2x10^4$	2.6	9.6x1014

4. Conclusions

In conclusion, the effect of Cu-doping concentration on the growth of Sb2S3 thin films was studied by preparing the pure and Cu-doped Sb2S3 films by chemical bath deposition followed by annealing at 250 ^{o}C. The un-doped Sb2S3 films showed orthorhombic crystal structure, compact and round-shaped grain morphology, a direct optical band gap of 1.7 eV, and high electrical resistivity.

By doping Cu up to 2 at% in the films, the crystallite size increased, the morphology becomes smooth and more compact, the direct optical band gag was 1.72 eV, and electrical resistivity was decreased. Further increasing the Cu-doping concentration from 4 to 8.7 at%, a CuSbS2 secondary phase was formed, the crystallinity was decreased, the microstructure was compact and fine-grained, and the direct optical band gap was 1.72 eV, electrical resistivity decreased and carrier concentration increased. Overall, the Cu-doping showed increased electrical properties of the Sb2S3, which is beneficial for applying these layers in solar cell fabrication.

Acknowledgement

This work was supported by the National Research Foundation of Korea (NRF) grant funded by the Korea government (MOE) (No. NRF-2017R1D1A3B03034243)

References

[1] K. Mandal, A. Mondal, J. Phys. Chem. Solids **51**, 1339 (1990).
[2] O. Savadogo, K. Mandal, Sol. Energy Mater. Sol. Cells **26**, 117 (1992).
[3] R. Mane, B. Sankapal, C. Lokhande, Thin Solid Films **353**, 29 (1999).
[4] J. Desai, C. Lokhande, Thin Solid Films **237**, 29 (1994).
[5] Y. C. Choi, D. U. Lee, J. H. Noh, E. K. Kim, S. I. Seok, Adv. Function. Mater. **24**, 3587 (2014).
[6] X. Wang, J. Li, W. Liu, S. Yang, C. Zhu, T. Chen, Nanoscale **9**, 3386 (2017).
[7] C. Ghosh, B. Varma, Thin Solid Films **60**, 61 (1979).
[8] M. Y. Versavel, J. A. Haber, Thin Solid Films **515**, 7171 (2007).
[9] C. Bhosale, M. Uplane, P. Patil, C. Lockhande, Thin Solid Films **248**, 137 (1994).
[10] L. Bhira, H. Essaidi, S. Belgacem, G. Couturier, J. Salardenne, N. Barreaux, J. Bernede, Phys. Status Solidi (a) **181**, 427 (2000).
[11] N. Yesugade, C. Lokhande, C. Bhosale, Thin Solid Films **263**, 145 (1995).
[12] S. Subramanian, D. P. Padiyan, et al., Phys. B: Cond. Matt. **405**, 925 (2010).
[13] I. Grozdanov, M. Ristov, G. Sinadinovski, M. Mitreski, J. Non-Cryst. Solids **175**, 77 (1994).
[14] M. Nair, Y. Pena, J. Campos, V. Garcia, P. Nair, J. Electrochem. Soc. **145**, 2113 (1998).
[15] H.-Y. Lee, J.-K. Kim, H.-B. Chung, J. Non-Cryst. Solids **279**, 209 (2001).
[16] B. Ismail, S. Mushtaq, A. Khan, Chalcogen. Let. **11**, 37 (2014).
[17] S. Mushtaq, B. Ismail, M. A. Zeb, N. S. Kissinger, A. Zeb, J. Alloy. Compd. **632**, 723 (2015).
[18] E. Cardenas, A. Arato, E. Perez-Tijerina, T. D. Roy, G. A. Castillo, B. Krishnan, Sol. Energy Mater. Sol. Cells **93**, 33 (2009).
[19] S. Ito, K. Tsujimoto, D.-C. Nguyen, K. Manabe, H. Nishino, Int. J. Hyd. Energy **38**, 16749 (2013).
[20] U. Chalapathi, B. Poornaprakash, C.-H. Ahn, S.-H. Park, Mater. Sci. Semicon. Proces. **84**, 138 (2018).
[21] V. Janosevic, M. Mitric, N. Bundaleski, Z. Rakocevic, I. L. Validzic, Prog. Photovolt.: Res. Appl. **24**, 704 (2016).
[22] U. Chalapathi, B. Poornaprakash, C.-H. Ahn, S.-H. Park, Appl. Surf. Sci. **451**, 272 (2018).
[23] P. Makreski, G. Petrusevski, S. Ugarkovic, G. Jovanovski, Vib. Spec. **68**, 177 (2013).
[24] R. Parize, T. Cossuet, O. Chaix-Pluchery, H. Roussel, E. Appert, V. Consonni, Mater. Des. **121**, 1 (2017).

[25] J. Baker, R. S. Kumar, D. Sneed, A. Connolly, Y. Zhang, N. Velisavljevic, J. Paladugu, M. Pravica, C. Chen, A. Cornelius, et al., J. Alloy. Compd. **643**, 186 (2015).
[26] V. Vinayakumar, S. Shaji, D. Avellaneda, T. D. Roy, G. Castillo, J. Martinez, B. Krishnan, Sol. Energy Mater. Sol. Cells **164**, 19 (2017).
[27] U. Chalapathi, B. Poornaprakash, C.-H. Ahn, S.-H. Park, Ceramic. Int. **44**, 14844 (2018).
[28] R. A. Garcia, C. M. Avenda~no, M. Pal, F. P. Delgado, N. Mathews, Mater. Sci. Semicond. Proc. **44**, 91 (2016).